Materials Letters 138 (2015) 179–183

Contents lists available at ScienceDirect

Materials Letters

journal homepage: www.elsevier.com/locate/matlet

Effect of Fe-doping on the structural, microstructural, optical, and ferroeletric properties of $Pb_{1/2}Sr_{1/2}Ti_{1-x}Fe_xO_3$ oxide prepared by spin coating technique

F.M. Pontes [a,*], D.S.L. Pontes [b], A.J. Chiquito [c], Marcelo A. Pereira-da-Silva [d,e], E. Longo [b,f]

[a] Department of Chemistry, Universidade Estadual Paulista—Unesp, PO Box 473, 17033-360 Bauru, São Paulo, Brazil
[b] LIEC—Department of Chemistry, Universidade Federal de São Carlos, Via Washington Luiz, Km 235, PO Box 676, 13565-905 São Carlos, São Paulo, Brazil
[c] NanO LaB—Department of Physics, Universidade Federal de São Carlos, Via Washington Luiz, Km 235, PO Box 676, 13565-905 São Carlos, São Paulo, Brazil
[d] Institute of Physics of São Carlos, USP, São Carlos 13560-250, São Paulo, Brazil
[e] UNICEP, São Carlos 13563-470, São Paulo, Brazil
[f] Institute of Chemistry, Universidade Estadual Paulista—Unesp, Araraquara, São Paulo, Brazil

ARTICLE INFO

Article history:
Received 30 July 2014
Accepted 1 October 2014
Available online 13 October 2014

Keywords:
Thin films
Ferroelectric properties
Optical properties
AFM
Perovskite

ABSTRACT

The influence of Fe content on the structural, microstructural, dielectric, ferroelectric and optical properties was investigated in $Pb_{1/2}Sr_{1/2}Ti_{1-x}Fe_xO_3$ films deposited on $Si/SiO_2/Ti/Pt$ and quartz substrates. X-ray diffraction showed that all films presented polycrystalline and single perovskite phases and the change of lattice parameters caused by increasing Fe-doping content replacing Ti^{4+} ions is very small to be detected by X-ray diffraction technique. Micro-Raman analysis showed the tetragonal nature for both undoped-PSTF and doped-PSTF (1%Fe) films, while both doped-PSTF (5%Fe) and PSTF-10 (10%Fe) films presented a pseudocubic structure. It was noticed that all films exhibited a homogeneous microstructure, compact and crack-free. The remnant polarization in the Fe-doped PSTF films was weaker than that for undoped-PSTF films which was attributed to structural changes and smaller grain size. The increasing of Fe content leads to a red shifted band gap relative to undoped PSTF films due localized levels within the forbidden band of PSTF.

1. Introduction

During the last decade, research on $PbTiO_3$ derived materials have resulted in a broad range of products with different applications for these materials [1–5]. It is well known that perovskite ABO_3-type $PbTiO_3$ (PTO) is an excellent ferroelectric oxide, which exhibit band gap about 3.4 eV, high tetragonal distortion and a high ferroelectric–paraelectric transition temperature around 763 K [6,7]. However, other systems have emerged as of great interest such as ABO_3-perovskite family oxide: in recent years, researchers have been conducting fruitful research on transition metals doped-ABO_3 perovskite-family oxide. Regarding doping with iron, it is relevant to mention that $BaTiO_3$, $SrTiO_3$ and $PbTiO_3$ perovskite-family oxides has been successfully used as subject of numerous studies. In this class of compounds this is an issue of technological and scientific importance [8–12]. For example, from optical properties of strontium titanate ferrite, $SrTi_{1-x}Fe_xO_{3-\delta}$, the bandgap energy was observed to move to higher energy region as iron content is increased [13]. Actually, doped $PbTiO_3$ oxides have been intensively studied and results point to remarkably different electronic structure and physical properties when Pb is replaced by Ca, Sr, Ba, La and Ti by Zr, Fe, Co, Cu, Ni, Mn, Al [11,14–22]. In addition, several groups reported that the defects and vacancies generated by doping using transition metal ions reduce the lattice distortion responsible for ferroelectricity. However, Palkar and Malik results seem not to be in agreement with lattice distortion reducing for $PbTi_{0.50}Fe_{0.50}O_{3-\delta}$ samples [11]. More recently, Verma et al. investigated the effect of Sr doping in $Pb_{1-x}Sr_x(Fe_{0.012}Ti_{0.988})O_3$ complex ceramics [23,24]. The authors reported that the tetragonal distortion and particle size have been reduced with increasing strontium concentration. Hence the combination of these doping materials at preferential sites A, B or both is essential to realizing practical perovskite-family oxide based functional devices as reported in literature.

In this report, we systematically investigate the effects of the different Fe-doping concentrations on the crystal structure, microstructure, dielectric, ferroelectric and optical properties of $(Pb_{1/2}Sr_{1/2})(Ti_{1-x}Fe_x)O_3$ samples synthesized by simple solution-based method, such as the chemical polymeric precursor method.

* Corresponding author. Tel.: +55 14 3103 6135; fax: +55 14 3103 6088.
E-mail address: fenelon@fc.unesp.br (F.M. Pontes).

http://dx.doi.org/10.1016/j.matlet.2014.10.005
0167-577X/

2. Experimental procedure

Strontium acetate, lead acetate, iron nitrate [$Fe(NO_3)_3 \cdot 9H_2O$], and titanium isopropoxide $Ti[OCH(CH_3)_2]_4$ were used for precursor materials of Sr, Pb, Fe, and Ti, respectively. Initially, $Ti[OCH(CH_3)_2]_4$ was dissolved in a mixture of deionized water and citric acid at 80 °C under stirring on magnetic stirrer. Separately, [$Fe(NO_3)_3 \cdot 9H_2O$] was dissolved in a mixture of deionized water and citric acid at 80 °C under stirring on magnetic stirrer. Then, the titanium–citrate and iron–citrate solutions were mixed at a stoichiometric quantity in order to produce a $Ti_{1-x}Fe_x$ solution at 80 °C under constant stirring. Then, lead acetate trihydrate was dissolved in deionized water, which was added into the $Ti_{1-x}Fe_x$ solution drop by drop under constant stirring to produce a Pb–Fe–Ti complex solution. After homogenization, strontium acetate was slowly added under constant stirring resulting in a clear Pb–Sr–Ti–Fe complex solution. In addition, a small amount of citric acid was added in order to increase the stability of the polymeric network structure. Finally, 40% by weight of ethylene glycol monomer was added on the basis of the final product of $(Pb_{1/2}Sr_{1/2})(Ti_{1-x}Fe_x)O_3$ complex solution. The solution was stirred constantly at 90 °C until a transparent and stable yellow precursor complex solution was obtained. This solution was more viscous but devoid of any visible phase separation. The precursor solution was deposited onto the Pt/Ti/SiO_2/Si and quartz substrates by spin coating at 6500 rpm for 20 s using a spinner (spin-coater KW-4B, Chemat Technology) via a syringe filter to avoid particulate contamination.

After spin coating, the samples were preheated at 200 °C for 10 min on a hot plate to remove residual solvent. Then, the thin films were annealed layer by layer at 400 °C/4 h and 700 °C/2 h in air to remove residual organic components and crystallization at a heating rate of 5 °C/min, respectively. The thin films were prepared by repeating the deposition and pyrolysis/crystallization cycle.

The phase structures of the $(Pb_{1/2}Sr_{1/2})(Ti_{1-x}Fe_x)O_3$ samples were identified using a Rigaku D/Max 2400 X-ray diffractometer ($CuK_\alpha = 1.54056$ Å radiation). Thin film thicknesses were characterized using a field-emission scanning electron microscopy (FE-SEM) (FEG-VP Zeiss Supra 35) with a secondary electron lens detector on a freshly fractured film/substrate cross-section. Surface microstructures of these samples were characterized using atomic force microscope (AFM). A Bruker Dimension ICON was used in these experiments. The optical transmittance of the $(Pb_{1/2}Sr_{1/2})(Ti_{1-x}Fe_x)O_3$ thin films were recorder in wavelength range from 200 to 3300 nm using a PerkinElmer Lambda 1050 spectrophotometer.

Raman measurements were taken with a T-64000 Jobin-Yvon triple-monochromator coupled to a charge-coupled device (CCD) detector. An optical microscope with a 100 × objective was used to focus the 514.5 nm line of a Coherent Innova 90 argon laser onto the sample. The power was maintained at 15 mW.

For electrical property measurements, circular Au electrodes were prepared by evaporation through a shadow mask with a 4.9×10^{-2} mm^2 dot area to obtain an array of capacitors. The deposition was carried out under vacuum (10^{-6} Torr). Ferroelectric and dielectric properties were undertaken using Premier Precision from Radiant Technology and Agilent 4294A Precision Impedance Analyzer, respectively, at room temperature.

3. Results and discussion

Fig. 1a shows the X-ray diffraction patterns of 0%, 1%, 5% and 10% Fe-doped PSTF-0, PSTF-1, PSTF-5 and PSTF-10 thin films on Si/SiO_2Ti/Pt substrates, respectively. All the films annealed at 700 °C show a single perovskite phase. No second phase pyrochlore was detected in these Fe-doped PSTF films indicating that Fe-doping concentration even up to 10% did not introduce any deleterious effects. The values of the lattice parameters of the PSTF films remained almost unchanged except for a small variation in the c/a ratio (1.0069, 1.0035, 1.0026 and 1.0013, corresponding to PSTF-0, PSTF-1, PSTF-5 and PSTF-10 samples, respectively). In addition, these results are similar to those observed by Ganegoda et al. [25], Sun et al. [14], in Fe-doped $PbTiO_3$ specimens and by Ye et al. [26], Gong et al. [27], in Fe-doped $Ba_{0.65}Sr_{0.35}TiO_3$ thin films.

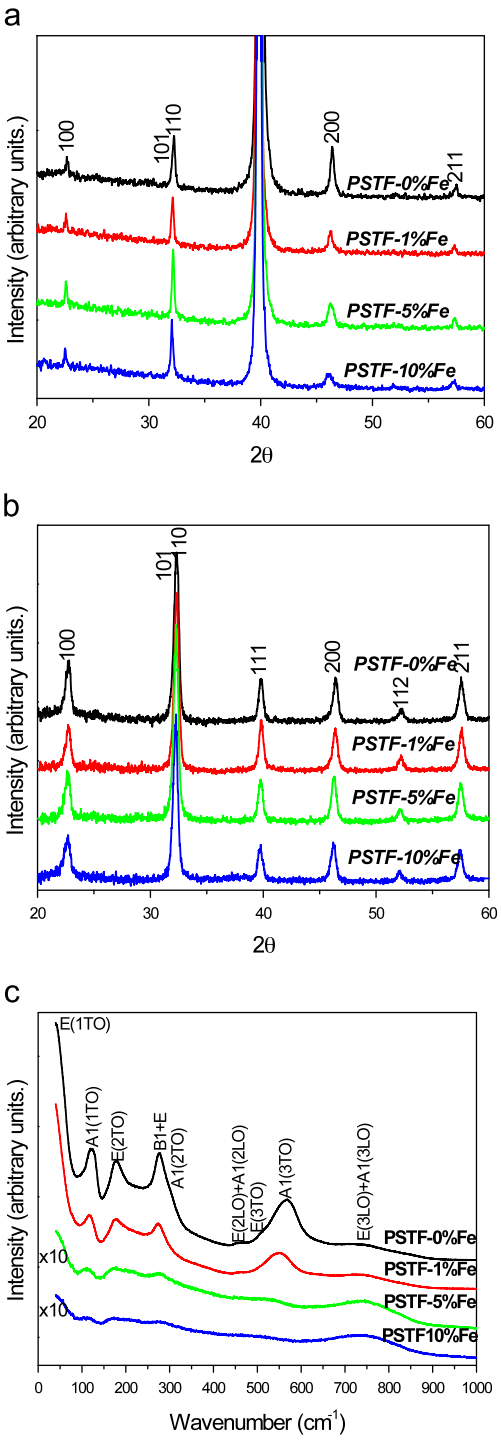

Fig. 1. (a) X-ray diffraction of Fe doped PSTF films deposited on Si/SiO_2/Ti/Pt; (b) quartz substrates and (c) micro-Raman spectra of Fe doped PSTF films deposited on Si/SiO_2/Ti/Pt substrate.

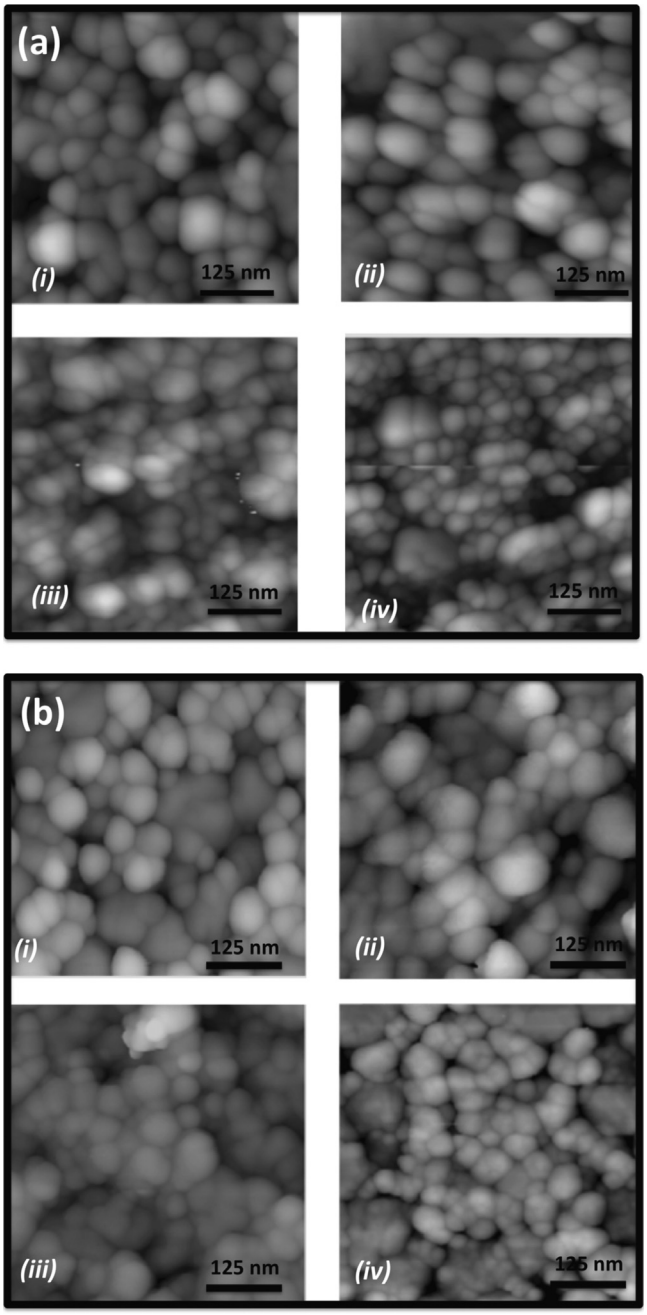

Fig. 2. Atomic force microscopy image of Fe doped PSTF films deposited on (a) Si/SiO_2/Ti/Pt and (b) quartz substrates. (i) PSTF-0; (ii) PSTF-1; (iii) PSTF-5 and (iv) PSTF-10.

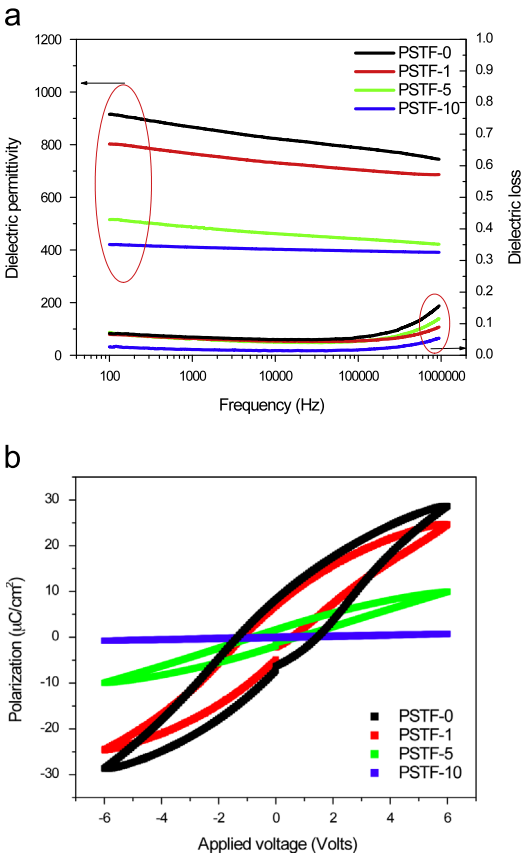

Fig. 3. (a) Frequency dependence of the dielectric permittivity and dielectric loss and (b) hysteresis loops of the PSTF-0, PSTF-1, PSTF-5 and PSTF-10 films on platinum bottom electrode.

In order to optical measurements Fig. 1b shows the X-ray diffraction patterns of 0%, 1%, 5% and 10% Fe-doped PSTF-0, PSTF-1, PSTF-5 and PSTF-10 thin films on quartz substrates, respectively. All thin films showed similar XRD patterns in comparison Fig. 1a. In Fig. 1c are shown Raman spectra of PSTF samples as a function of Fe-doping. The PSTF-0 thin films obtained by treatment at 700 °C show strong bands at 121, 178, 277, 459, 566, and 736 cm^{-1}, corresponding to tetragonal PSTF-0 structure as seen in Fig. 2. In contrast, Fe-doped PSTF-1 thin films show similar Raman spectra but the wavelength peak positions are slightly shifted toward lower frequencies for A1(1TO) and A1(3TO) modes (at 116 and 546, respectively), suggesting a reduction to the tetragonal lattice. Surprisingly, the Raman spectra of the Fe-doped PSTF-5 and PSTF-10 thin films show lower and broad intensity peaks (or shoulders) at 105, 176, 277, 520 and 736 cm^{-1}. In addition, the strong A1(3TO) band at 566 cm^{-1} which is observed in PSTF-0 and PSTF-1 is almost absent in PSTF-5 and PSTF-10 thin films. From these results, it seems that Fe ions substituting Ti^{4+} ions into BO_6 lattice undergo a drastic short- and medium-range structural change. Thus, Raman studies confirmed that both PSTF-5 and PSTF-10 samples might be assigned to pseudocubic phase.

Fig. 2 show the surface morphology from atomic force microscopy for the 0%, 1%, 5% and 10% Fe-doped PSTF films deposited on Si/SiO_2/Ti/Pt and quartz substrates after annealing at 700 °C, respectively. It can be observed that the all PSTF films exhibit a rather relatively smooth, precipitates-free and dense surfaces, spherical grains morphologies and crack-free, indicating the good quality of the PSTF films. The estimated values of grain sizes from the AFM images of PSTF-0, PSTF-1, PSTF5 and PSTF-10 films on Si/SiO_2/Ti/Pt substrate are 66, 54, 42 and 35 nm, respectively.

The dielectric and ferroelectric properties of the PSTF films were investigated as a function of the Fe doping, Fig. 3a and b, respectively. The PSTF films thicknesses were measured to be approximately 260, 250, 340 and 330 nm for PSTF-0, PSTF-1, PSTF-5 and PSTF-10 films, respectively. Fig. 3a shows the frequency dependence of the dielectric permittivity and dielectric loss ranging from 10^2 to 10^6 Hz of the films, measured at room temperature. These results show that the dielectric permittivity response decreases significantly as the Fe doping level increases. It can also be observed that the dielectric loss of all Fe-doped films are slightly smaller than that for undoped PSTF films. The values of dielectric permittivity and dielectric loss measured at a frequency of 100 kHz were 788, 704, 442, 396 and 0.056, 0.045, 0.044, 0.016 for PSTF-0, PSTF-1, PSTF-5 and PSTF-10 films, respectively. A possible scenario for the dielectric permittivity decrease at higher

Fe-doping concentration is given in the following. It is well known and reported in literature that (1) the intrinsic oxygen vacancies normally occur in the $ABO_{3-\delta}$ perovskite-family structure (see Eqs. (1) and (2)) when doping ion contains a valence lower than the ion at the B site, extrinsic oxygen vacancies with positive charge are found to occur (see Eq. (2)).

$$O_O^x \leftrightarrow V_O^{\bullet\bullet} + 2e' + 1/2O_{2(g)} \quad (1)$$

$$Fe_{Ti}^x \leftrightarrow 2Fe_{Ti}' + V_O^{\bullet\bullet} + 1/2O_{2(g)} \quad (2)$$

In this approach, the extrinsic oxygen vacancy in PSTF films may exceed the intrinsic oxygen vacancy due higher Fe concentration in the perovskite phase structure; so the excess of extrinsic oxygen vacancies can be deleterious to the dielectric properties. In contrast, when Fe^{3+} substitutes Ti^{4+}, Fe_{Ti}' extrinsic defects behave as electron acceptors in the perovskite structure and they can effectively reduce the dielectric loss. Fig. 3b shows the ferroelectric polarization for PSTF films at room temperature. In the present case, it can be observed that an increase in Fe content leads to a remnant polarization decrease, indicating a reduction of ferroelectricity. Under applied voltage of 6V, 0%, 1%, 5% and 10% Fe-doped PSTF films presented remanent polarization (P_r) values around of 8.5, 6.5, 1.5 and 0.2 μC/cm^2, respectively. This behavior may be attributed to the following: (i) reduction of the average grain size with increasing Fe concentration, (ii) the more Fe-doping concentration, the smaller tetragonal distortion as observed in Raman data, (iii) when the Fe-doping level is up to 5%, the acceptor Fe-doping causes significant increase in extrinsic oxygen vacancy concentration which in turn, results in the decrease of polarization.

The optical properties of the PSTF films with different proportion of Fe-doping ion deposited on quartz substrates were investigated by recording transmission response in a wide region, from 200 to 3300 nm. All prepared films were highly transparent from UV–visible/near infrared region as seen in Fig. 4a. As Fe doping level increased, replacing Ti^{4+} ions, a shift of the fundamental optical absorption edge to high wavelength occur, indicating a decrease of the band gap energy. The magnified view of the spectrum in 200–800 nm range (inset of Fig. 4a) clearly exhibits this red shift. In addition, the band gap energies of the PSTF films were estimated by the Tauc's law described as [28]:

$$\alpha h\nu = A(h\nu - E_g)^n, \quad (3)$$

where n is a constant which characterizes different types of transition ($n=1/2$, 3/2, 2 or 3 for allowed direct, forbidden direct, allowed indirect, and forbidden indirect, respectively), h is the Planck constant, ν is the photon frequency, $h\nu$ is the incident photon energy, α is the absorption coefficient, A is a constant and E_g is the band gap energy value. Thus, the dependence of $(\alpha h\nu)^n$ versus incident photon energy ($h\nu$) yields the band gap E_g value. As depicted in Fig. 4b, the relationship between $(\alpha h\nu)^2$ plotted against ($h\nu$) varies linearly in the high energy region of the absorption edge, which is consistent with a direct band gap. The band gap energies were found to be 3.74, 3.61, 3.48 and 3.32 eV for PSTF-0, PSTF-1, PSTF-5 and PSTF-10 films, respectively. As can be noted, the PSTF band gap energies decrease with increase of the Fe doping level. This a direct consequence of the change of the band structure (electronic states) from the undoped PST to the doped PSTF samples. According to band-structure calculations, the energy band gap of (Pb,Sr)TiO_3 (PST) crystal is determined by the difference between the conduction band, mainly constituted by Ti 3d orbitals and by valence band, mainly described by O 2p orbitals. Therefore, the impurity states due to oxygen vacancies and 3d Fe doping levels play an important role in the formation of the band structure, with the introduction of localized bands within the original band gap of PST crystal. These localized states induced

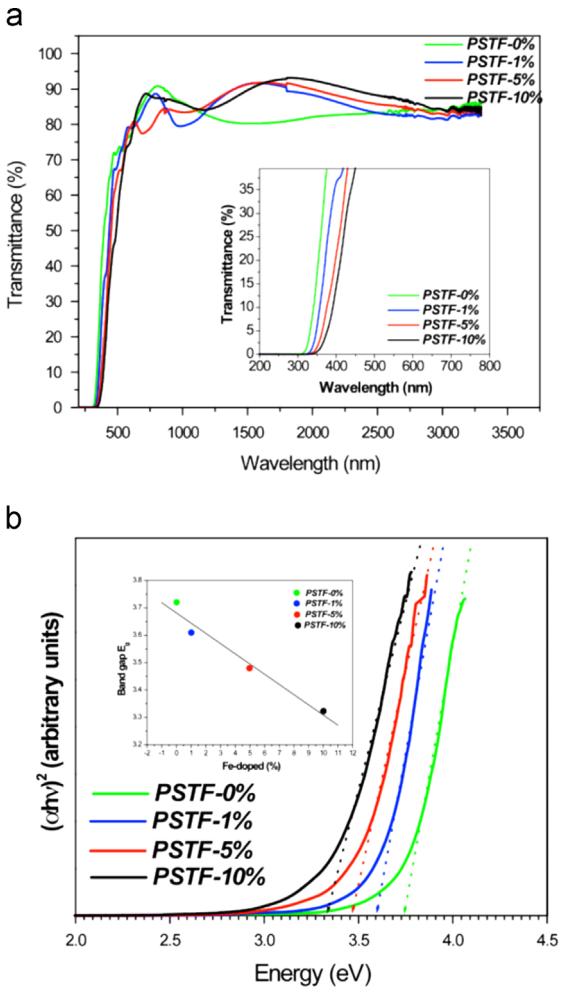

Fig. 4. (a) Optical transmission spectra of the PSTF-0, PSTF-1, PSTF-5 and PSFT-10 films on quartz substrate and (b) plots of $(\alpha h\nu)^2$ versus ($h\nu$) for PSTF-0, PSTF-1, PSTF-5 and PSFT-10 films on quartz substrate. The optical band gap energy E_{gap} is obtained by extrapolation of the linear region for $(\alpha h\nu)^2=0$.

by Fe-doping are expected to form deep and/or shallow levels, leading to a significant decrease in band gap energy. Insulating perovskites present semiconducting or metallic character depending on the presence of defects (mainly oxygen vacancies) or doping. Oxygen vacancies act as donor centers resulting in n-type semiconductors with the Fermi level near to the bottom the conduction band. Fig. 5 depicts a sketch of the electronic configuration of PST films when in presence of doping or vacancies. There is a band gap narrowing in both cases but we believe that Fe doped samples should present a lower band gap due to the contribution of Fe orbitals to both valence and conduction bands. Similar behavior of the optical band gap has been reported in the literature by Tin et al. in Ba(Mn_xTi_{1-x})O_3 thin films [29]. It was found a strong dependence of the optical band gap on Mn/Ti ratios. Recently, other researchers have observed the decreasing of the optical band gap by increasing the transition metal doping [30–32]. In addition, there is an approximately linear relation between band gap energy and Fe-doping level (inset Fig. 4b), similar to what happens in classical semiconductor alloys [33].

4. Conclusion

In conclusion, $Pb_{1/2}Sr_{1/2}Ti_{1-x}Fe_xO_3$ films with different Fe-doping levels were successfully prepared by spin coating

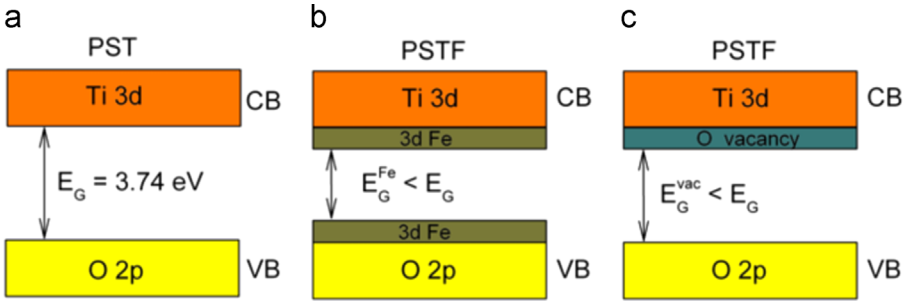

Fig. 5. (a) simplified band diagram for PST films. The band gap was estimated from the Tauc's law. Band gap narrowing due to Fe doping and to the presence of vacancies are sketched in panels (b) and (c), respectively.

technique on $Si/SiO_2/Ti/Pt$ and quartz substrates. X-ray diffraction structural analysis suggests that all films are pure perovskite structure with random crystalline orientation. A deep investigation of the crystal structure by Raman spectroscopy showed drastic changes in bands intensity, phonon positions, line widths as a function of increasing Fe doping levels. These results strongly suggest a change short- and medium-range structural order parameter, a direct evidence of a possible structural phase transition from tetragonal-to-pseudocubic at room temperature. Increasing the Fe doping level the PSTF films exhibits weak ferroelectric properties (attributed to smaller tetragonal distortion), a decrease in grain sizes and a large contribution from oxygen vacancies. The optical transmittance studies revealed that all films are highly transparent from 400 to 3300 nm while a red shift was observed in the typical spectra. Also it was observed a decrease in band gap energies as a function of Fe doping level. It is a consequence of the modification of the band structure due the inclusion of localized states into the forbidden band. The present studies reveal that the adjusting structural, microstructural, dielectric, ferroelectric and band gap properties can be achieved by controlling the Fe-doping content accurately in $Pb_{1/2}Sr_{1/2}Ti_{1-x}FeO_3$ complex oxide.

Acknowledgments

This work was financially supported by the Brazilian agencies FAPESP and CNPq. We thank CEPID/CDMF/INCTMN. FAPESP process nos. 08/57150-6, 11/20536-7, 12/14106-2 and 13/07296-2. INCTMN process no 08/57872-1. CNPq process no 573636/2008-7.

References

[1] Dippel AC, Schneller T, Dornseiffer J, Waser R. J Sol-Gel Sci Technol 2011;57:36–42.
[2] Jegatheesan P, Yadav HK, Gupta V, Giridharan NV. Mater Lett 2011;65:901–4.
[3] Tyunina M, Levoska J, Leppavuori S, Shorubalko R, Sternberg A. J Appl Phys 2000;88:4274–81.
[4] Singh A, Choudhary I, Mehta S, Dahiya S, Walia CS, Raina KK, et al. J Appl Phys 2010;107 (084106-4).
[5] Fu M, Chi QG, Wang X, Chen Y, Lei QQ. Mater Lett 2012;80:20–2.
[6] Zhu J, Zhang J, Xu H, Vogel SC, Jin C, Frantti J, et al. Sci Rep 2014;4:1–6.
[7] Mansoor MA, Ismail A, Yahya R, Arifin Z, Tiekink ERT, Weng NS, et al. Inorg Chem 2013;52:5624–6.
[8] Sahner K, Gouma P, Moos R. Sensors 2007;7:1871–86.
[9] Mishra A, Mishra N. Int J Mater Sci Appl 2012;1:14–21.
[10] Erdem E, Jakes P, Parashar SKS, Kiraz K, Somer M, Rudiger A, et al. J Phys Condens Matter 2010;22:345901–7.
[11] Palkar VR, Malik SK. Solid State Commun 2005;134:783–6.
[12] Palkar VR, Purandare SC, Gohil S, John J, Bhattacharya S. Appl Phys Lett 2007;90:172901–3.
[13] Ghaffari M, Liu T, Huang H, Tan OK, Shannon M. Mater Chem Phys 2012;136:347–57.
[14] Sun C, Wang J, Kang H, Chen J, Kimb MJ, Xing X. Dalton Trans 2010;39:9952–5.
[15] Shuklan A, Choudhary RNP. Physica B 2010;405:2508–15.
[16] Palkar VR, Purandare SC, Ayyub P, Pinto R. J Appl Phys 2000;87:462–6.
[17] Reddy KH, Parida K. ChemCatChem 2013;5:3812–20.
[18] Katna AK, Kotnala RK, Negi NS. Physica B 2013;425:95–9.
[19] Boland SW, Pillai SC, Yang WD, Haile SM. J Mater Res 2004;19:1492–8.
[20] Pontes FM, Leal SH, Pizani PS, Santos M R M C, Leite ER, Longo E, et al. J Mater Res 2003;18:659–63.
[21] Pontes DSL, Pontes FM, Marcelos A Pereira-da-silva, Zampieri M, Chiquito AJ, Pizani PS, et al. Ceram Int 2014;40:4085–93.
[22] Stoupin S, Chattopadhyaya S, Bolin T, Segre CU. Solid State Commun 2007;144:46–9.
[23] Verma KC, Negi NS. Scr Mater 2010;63:891–4.
[24] Verma KC, Ram M, Kotnala RK, Bhatt SS, Negi NS. Indian J Pure Appl Phys 2010;48:593–9.
[25] Ganegoda H, Kaduk JA, Segre CU. Powder Diffr 2013;28:254–61.
[26] Ye Y, Guo T. Ceram Int 2009;35:2761–5.
[27] Gong J, Cheng J, Zhu W, Yu S, Wu W, Zhongyan M. IEEE Trans Ultrason Ferroelectr Freq Control 2007;54:2579–82.
[28] Tauc J, Menth A. J Non-Cryst Solids 1972;8:569–85.
[29] Ting Z, Jiang Y, Hong DL, Feng ZW. Chin Phys B 2013;11:117801–5.
[30] Yang J, Zhang T, Ni M, Ding L, Zhang WF. Appl Surf Sci 2009;256:17–20.
[31] Li YW, Sun JL, Meng XJ, Chu JH, Zhang WF. Appl Phys Lett 2004;85:1964–6.
[32] Dang NV, Nguyen HM, Chuang PY, Thanh TD, Lam VD, Lee CH, et al. Chin J Phys 2012;50:262–70.
[33] Schubert EF. Doping in III-V semiconductors. Cambridge: Cambrige University Press; 1993.